FORECASTERS' FORUM

Supercells in Environments with Atypical Hodographs

DAVID O. BLANCHARD

NOAA/National Weather Service, Flagstaff, Arizona

(Manuscript received 2 February 2011, in final form 19 June 2011)

ABSTRACT

An unusual severe weather event with supercell thunderstorms developed across portions of northern Arizona in the midst of the warm-season North American monsoon—a regime characteristically dominated by a subtropical upper-level high over the southwestern United States. The approach of a midlatitude, cold-core, upper-level low brought an environment of enhanced shear and increased instability supportive of supercells. This atypical system is described and how a correct interpretation of the winds and hodograph would allow a forecaster to maintain situational awareness is discussed.

1. Introduction

Occurrences of supercell thunderstorms producing widespread severe weather in northern Arizona are most likely to arise during the transition between the moist, subtropical environment of the warm-season North American monsoon regime (NAM; Adams and Comrie 1997) and the first, early season incursions of midlatitude baroclinic systems. The presence of copious tropical moisture, combined with steeper lapse rates, increased buoyant instability, and, more importantly, deep-layer shear, is supportive of supercells, which are responsible for most of the severe weather. The transition season typically occurs during September but can occur as late as October (Blanchard 2006).

The atmospheric environment that developed across northern Arizona during the afternoon and early evening of 14 August 2003 resulted in an unusual severe weather episode. Although it was in the midst of the warm-season NAM—characteristically dominated by a sprawling subtropical upper-level high over Mexico and the southwestern United States—a midlatitude, cold-core, upper-level low approached from the east-northeast and moved toward Arizona. The combination of enhanced deep-layer shear associated with the approaching cyclonic circulation, and the ever-present deep moisture and buoyant instability associated with the NAM, produced numerous severe supercell thunderstorms over the area.

Examination of the winds aloft indicated that the hodograph shape retained the anticyclonic (i.e., clockwise) curvature associated with classical severe weather hodographs (Maddox 1976; Doswell 1991; Brown 1993; Bunkers et al. 2000); however, the hodograph was rotated clockwise approximately three octants from the more classical orientation. The deep-layer mean wind and shear associated with this wind profile resulted in convective storms that moved toward the southwest with right-mover (RM) supercells attaining a more westerly motion and left-mover (LM) supercells a more southerly motion.

The focus in this short presentation is on examining the vertical structure of the wind field associated with the midlatitude, cold-core, upper-level low through the use of observed and model forecast hodographs and to show how an operational forecaster might make use of this information to be situationally aware regarding the development of supercellular convection under these atypical wind regimes within the NAM environment. Section 2 discusses the evolution and track of the upper-level low, section 3 discusses the shear and stability parameters, and a summary and discussion are found in section 4.

2. Origins of the upper-level low

The upper-level low that approached Arizona had its origins over the midwestern United States several days earlier. High pressure over the western United States

Corresponding author address: David O. Blanchard, NOAA/National Weather Service, P.O. Box 16057, Bellemont, AZ 86015. E-mail: david.o.blanchard@noaa.gov

DOI: 10.1175/WAF-D-11-00012.1

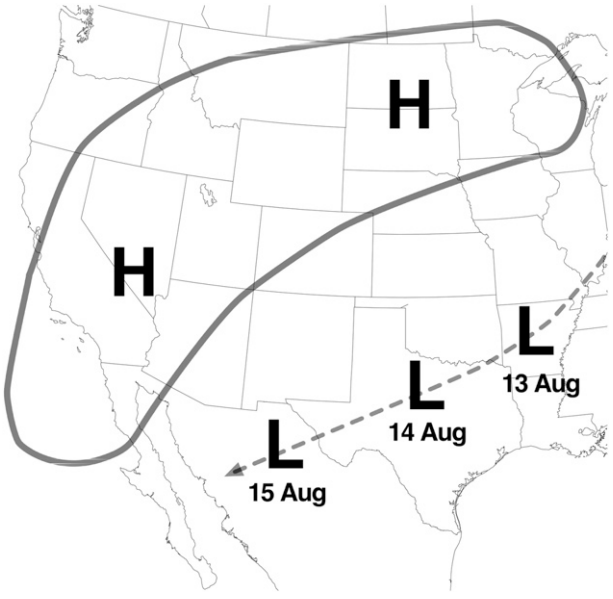

FIG. 1. The 500-mb location of the migrating upper-level low at 0000 UTC each day during the period 13–15 Aug 2003.

steered the cutoff upper-level low to the south toward the Gulf of Mexico and then southwestward across New Mexico and toward Arizona (Fig. 1). It should be noted that the operational forecast models correctly depicted this pattern of behavior and gave forecasters several days advance notice of an atypical situation. Pytlak et al. (2005) observed that in both 2003 and 2004 a few upper-level cyclonic-circulation systems originated in the polar westerlies and became wrapped underneath the subtropical ridge and then were entrained in the tropical easterlies. Previous work by Whitfield and Lyons (1992) reported that some of the lower-latitude upper-tropospheric cyclonic circulations had their origins in the midlatitude westerlies and that cold-air injection into the upper-cold low from midlatitudes via equatorward-penetrating upper-tropospheric troughs was not uncommon. Further, they showed that these systems were often collocated with enhanced convection as far west as Arizona and California and were occasionally associated with copious amounts of rain in the desert Southwest.

The 500-mb geopotential height field (Fig. 2) indicates that the center of the upper-level low was located along the Texas–Mexico border with minimum heights of 586 dam. North of this low was an upper-level high sprawling from southern California to the Great Lakes region with maximum geopotential heights of 598 dam. A narrow band of stronger winds was located between these two features from southeastern Colorado to northwestern New Mexico and then across east-central Arizona.

With its origins in the weakly baroclinic westerlies, the thermal structure of this system remained ''cold core.'' This resulted in steeper lapse rates and, consequently, greater buoyant instability than is characteristically observed in the desert Southwest during the NAM season when the area is dominated by a warm-core upper-level high with nearly moist-adiabatic lapse rates.

3. Stability and shear parameters

a. Sounding data

Temperature and moisture profiles are shown in the skew T–log$p$ plots for Flagstaff, Arizona (Fig. 3). The 1200 UTC (0500 LT) profile shows a classic ''onion'' sounding (Zipser 1977), typical of an environment in the wake of deep, moist convection (i.e., a marked stable layer separates cool, nearly saturated air near the surface from very warm and dry air above, once again becoming nearly saturated near and below the anvil region).[1] However, with the approach of the upper-level low, the 0000 UTC (1700 LT) sounding shows that the environment experienced drying aloft, slight moistening in the lower levels, and a steepening of the lapse rate in response to the cool air aloft. The wind profile shows both veering of the winds with height and moderate shear through a deep layer, characteristics not typically found in a summertime sounding at this location.

Convective available potential energy (CAPE) was calculated as described in Blanchard (1998) and repeated here. First, the mean mixing ratio ($\overline{w}$) in the lowest 1000 m was computed. From this value, the convective condensation level (CCL) and convective temperature (T_c) were determined. Parcels were assumed to have attained T_c with moisture $\overline{w}$. These parcels were lifted dry adiabatically to the CCL, then moist adiabatically to the equilibrium level. Surface-based CAPE (SBCAPE) was evaluated using the surface T and w. Both CAPE and SBCAPE employed the virtual temperature correction (AWS 1961, 1979; Doswell and Rasmussen 1994).

The 1200 UTC sounding had a CAPE of 195 J kg^{-1} with convective inhibition (CIN) of 150 J kg^{-1}; SBCAPE was 815 J kg^{-1} with CIN of 130 J kg^{-1}. At 0000 UTC, the CAPE had increased to 945 J kg^{-1} with CIN of 135 J kg^{-1}; SBCAPE was 2185 J kg^{-1} with no CIN.

Storm relative helicity (SRH; Davies-Jones et al. 1990) has been shown to be a measure of the potential for updraft rotation in supercells. Supercell storm motion[2] for determining SRH was derived using the methodology of Rasmussen and Blanchard (1998, hereafter RB98). The

[1] In fact, mesoscale convection had developed over northeastern Arizona and moved southwestward overnight.

[2] A forecast motion was used since this is typically what is available in an operational forecast environment.

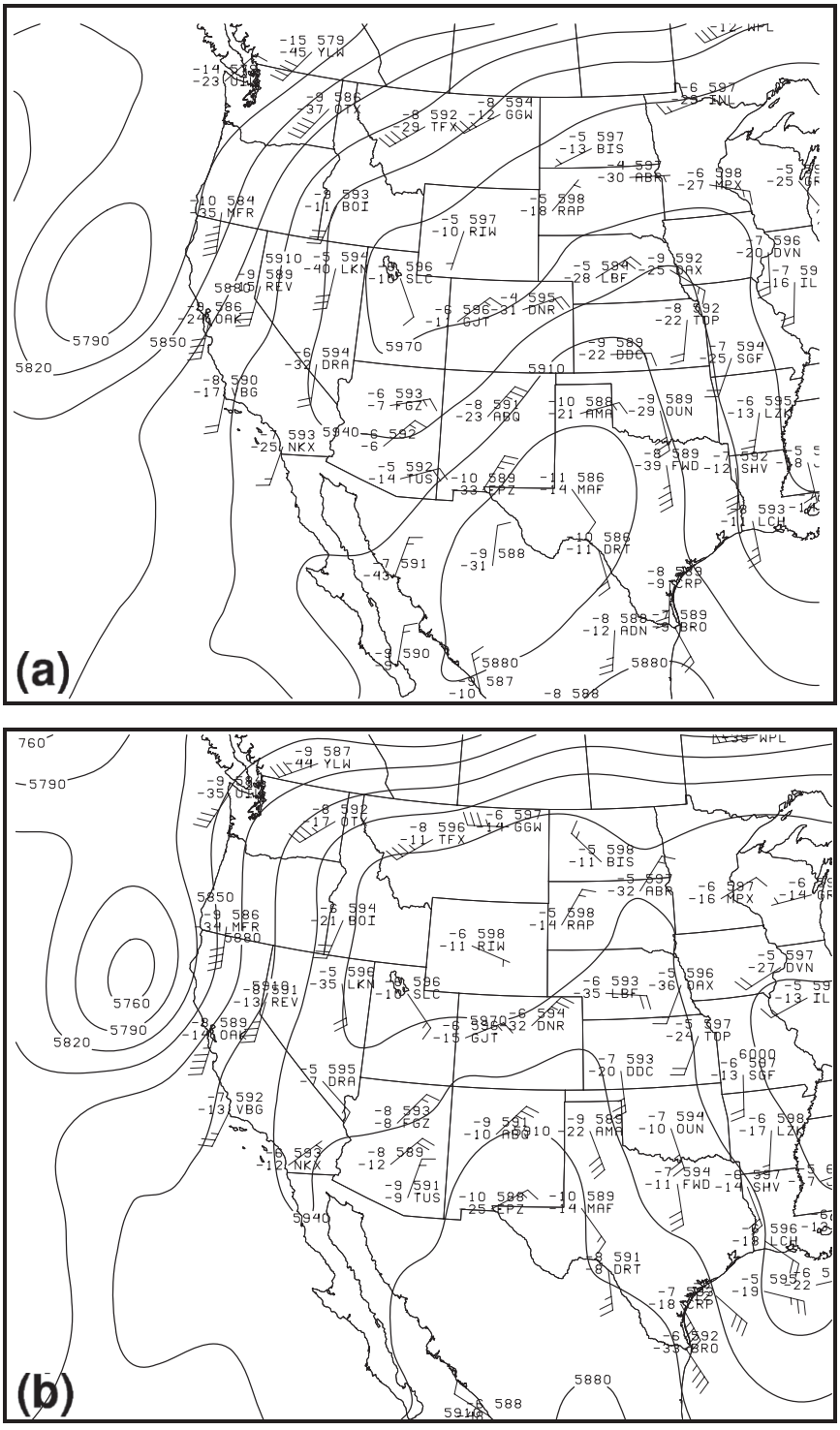

FIG. 2. Geopotential height and station data at 500 mb at (a) 1200 UTC 14 Aug and (b) 0000 UTC 15 Aug 2003. Height contours (solid lines) are every 30 m. Station data are plotted using standard conventions.

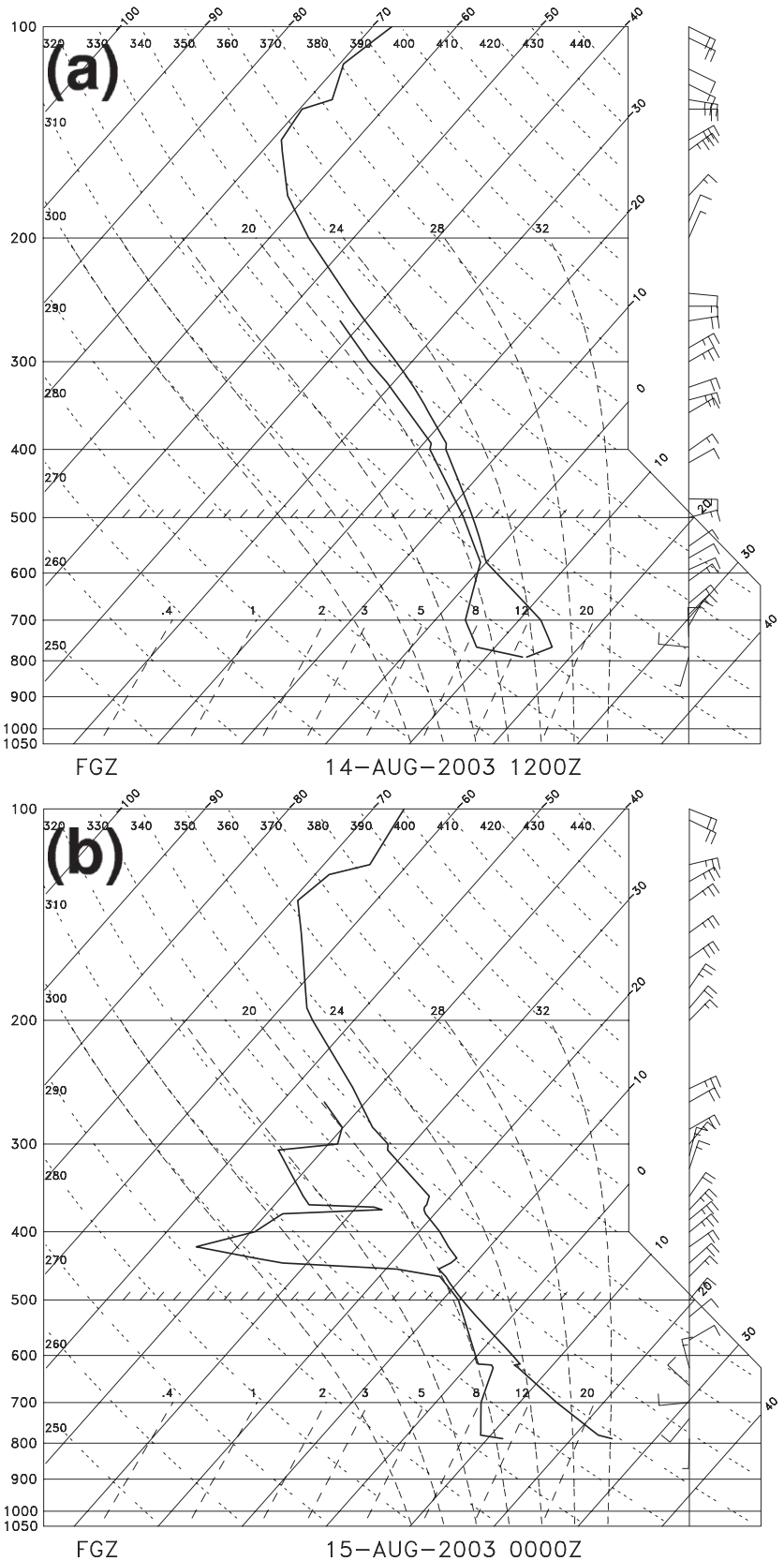

FIG. 3. Skew *T*–log*p* profile taken at KFGZ at (a) 1200 UTC 14 Aug and (b) 0000 UTC 15 Aug 2003. Winds are in m s^{-1} (half barb = 2.5 m s^{-1}; full barb = 5 m s^{-1}).

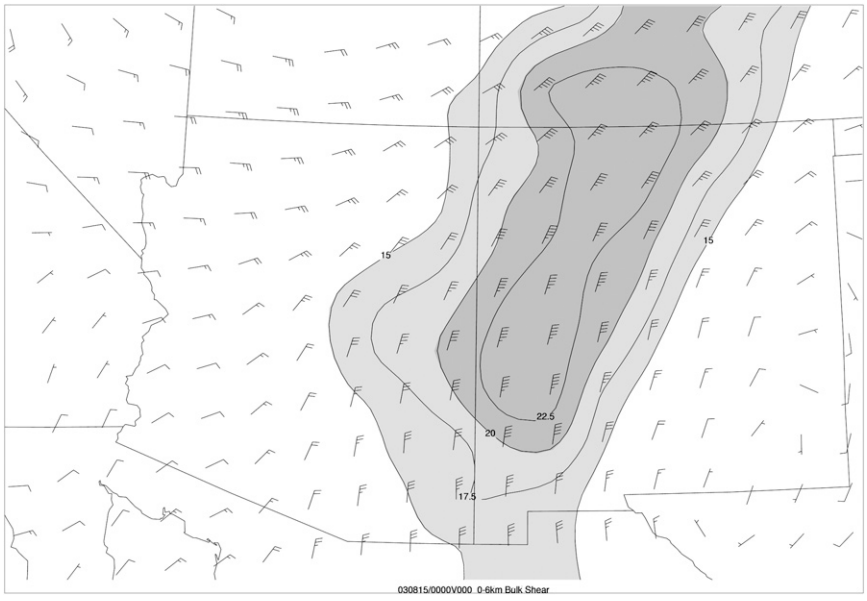

FIG. 4. Deep-layer 0–6-km bulk shear at 0000 UTC 15 Aug 2003. Contours (solid lines) shown every 2.5 m s^{-1} starting at 15 m s^{-1}; gray-fill pattern shown at 15 and 20 m s^{-1}. Winds are in m s^{-1} (half barb = 2.5 m s^{-1}; full barb = 5 m s^{-1}).

$SRH_{0–3}$ (SRH in the 0–3-km layer) was 155 m^2 s^{-2} at 1200 UTC, increasing to 175 m^2 s^{-2} by 0000 UTC. These values are significantly above the median for supercells but below the median for tornadoes given in RB98.

Bulk shear is the magnitude of the bulk wind vector difference [0–6 km is used here although other depths have been suggested; e.g., Houston et al. (2008)] and has been shown to be a strong discriminator between nonsupercell and supercell thunderstorms (Weisman and Klemp 1982, 1984; RB98; Thompson et al. 2003). The bulk shear was only 9 m s^{-1} at 1200 UTC but had increased to 15 m s^{-1} by 0000 UTC, which is only slightly less than the median value for both the supercell and tornado categories of RB98.

The vorticity generation parameter (VGP; RB98) was derived from an examination of the parameter space investigated in Rasmussen and Wilhelmson (1983) and the physical concept of tilting of vorticity. The rate of conversion of horizontal to vertical vorticity through tilting can be parameterized as the product of the mean shear and the square root of CAPE. VGP was small at 1200 UTC owing to the low values of CAPE but by 0000 UTC had increased to 0.2, which is close to the median value found by RB98 for supercells.

b. Gridpoint data

Gridpoint data from the Eta numerical forecast model (Black 1994) were also used to examine the wind field associated with this system. Figure 4 shows the deep-layer bulk shear (i.e., the 0–6-km layer). There is a region with bulk shear greater than 20 m s^{-1} in western New Mexico, with an extensive region greater than 15 m s^{-1}.

Eta Model analyses of $SRH_{0–3}$ indicated a broad band of higher values that oriented from the northeast to southwest from northwestern New Mexico across east-central Arizona (Fig. 5). Peak values were generally 150–200 m^2 s^{-2}. This compares favorably with the values found by RB98 for supercells and tornadic storms.

Figure 6 is an idealized schematic of a hodograph with anticyclonic curvature (i.e., winds veering with height). This hodograph has been rotated approximately three octants in the clockwise direction from the hodograph typically found in midwestern supercell environments. In the right half of Fig. 6 is a schematic representation of a radar depiction of a supercell (Lemon and Doswell 1979; Doswell and Burgess 1993) rotated clockwise the same amount. Note that this rotation results in the "hook echo" being located in the northwestern quadrant of the storm.

Both theoretical and modeling studies (Rotunno and Klemp 1982, 1985; Weisman and Klemp 1982, 1984) have demonstrated that the internal processes that produce supercell motion and characteristics depend on properties of the vertical wind shear, and not just the mean wind. Thus, the rotated or transformed wind profile and associated hodograph should result in supercell storms exhibiting similar characteristics to storms in the more common or typical hodograph, albeit with a different motion vector.

Figure 7 is a hodograph from Bellemont, Arizona (KFGZ), for the late afternoon period [0000 UTC (1700 LT) 15 August]. Initial storm motion from this

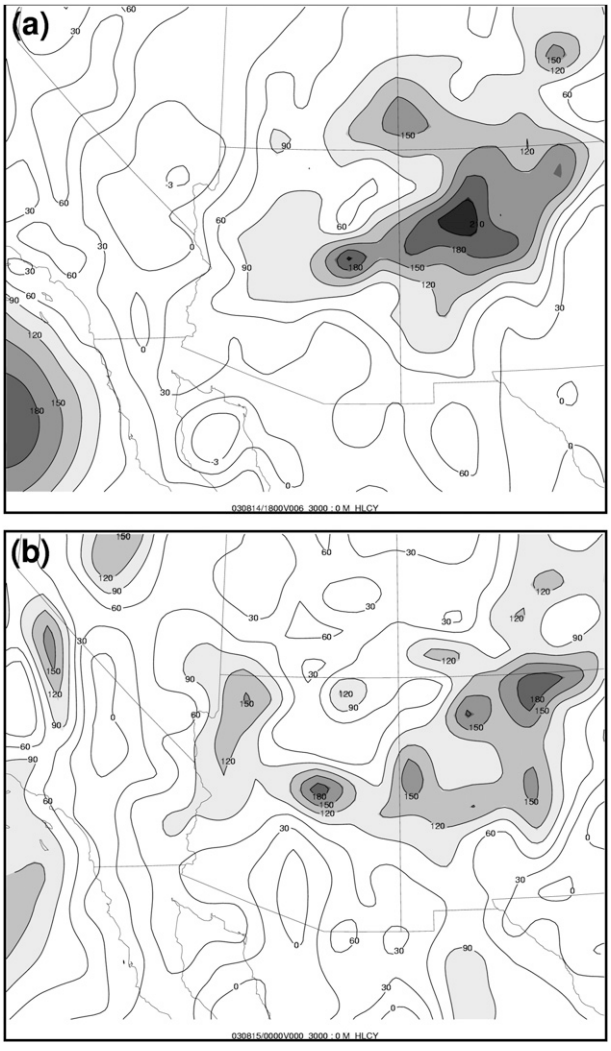

FIG. 5. The SRH_{0-3} at (a) 1800 UTC 14 Aug and (b) 0000 UTC 15 Aug 2003. Contours (solid lines) are shown every 30 $m^2 s^{-2}$; gray-fill pattern shown every 30 $m^2 s^{-2}$ starting at 90 $m^2 s^{-2}$.

hodograph would be to the southwest (050° at 10 m s^{-1}). Once a supercell thunderstorm begins to deviate to the right, its motion would be more westerly (084° at 10 m s^{-1}; RB98)[3] and the hook echo would be located in the right-rear (i.e., northwest) quadrant of this storm. Inspections of the Flagstaff (KFSX) Weather Surveillance Radar-1988 Doppler (WSR-88D) imagery and animations showed that the initial storms were moving from the northeast to the southwest as suggested by the sounding winds and hodograph. As the stronger storms acquired supercell characteristics, RM supercells moved

[3] The methodology of Bunkers et al. (2000) produces a right-moving supercell motion of 092° at 10 m s^{-1}.

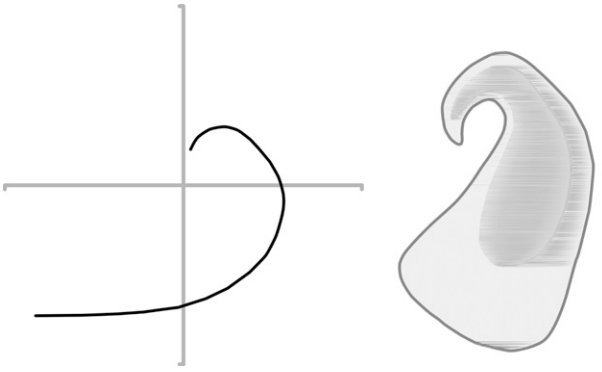

FIG. 6. (left) Idealized schematic of a hodograph typical of supercell environments and (right) a schematic representation of a radar depiction of a supercell. Both schematics are rotated clockwise approximately three octants from the more typical orientation of midwestern, springtime, supercell environments.

to the west-southwest while a few LM supercells moved to the south. Actual RM storm motions ranged from 068° to 082° at speeds of 10–25 m s^{-1} with a vector mean motion of 074° at 10 m s^{-1}. Variations in supercell storm motion were likely attributable to storm–storm and storm–outflow interactions (Weaver 1979; Zeitler and Bunkers 2005) and, possibly, variations in terrain.

Figure 8 shows the radar reflectivity from a well-developed supercell at 2353 UTC (1653 LT). There is a hook echo located on the northwestern flank of the RM

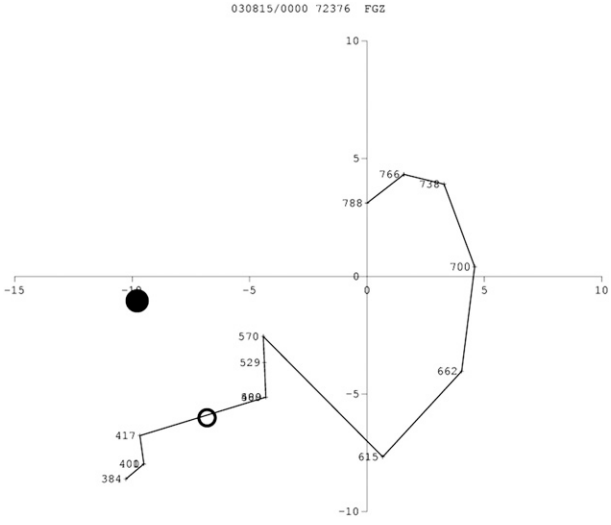

FIG. 7. Surface (788 mb) to 384-mb hodograph from KFGZ sounding valid at 0000 UTC 15 Aug 2003. The horizontal axis is the u component of the wind, vertical axis is the v component of the wind, and axes are in m s^{-1}. Tick marks are shown every 5 m s^{-1}. Numbers denote pressure levels for various points on the hodograph. Solid circle is the computed motion for an RM supercell; the open circle is the mean wind.

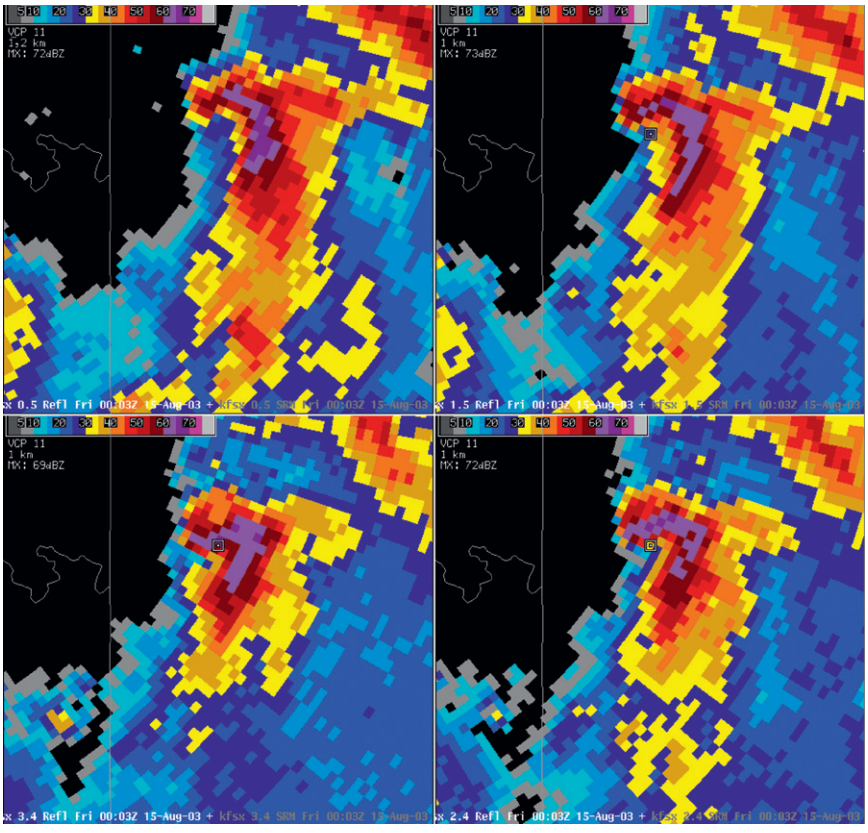

FIG. 8. Radar images from the KFSX radar at 0003 UTC 15 Aug 2003 showing reflectivity at tilts of (top left) 0.5°, (top right) 1.5°, (bottom right) 2.4°, and (bottom left) 3.4°. Color table for reflectivity values (dBZ) is shown in the top left of each image.

storm. Figure 9 shows the (ground relative) velocity field with a well-defined velocity couplet at the same location as the hook echo. Other storms that developed on this day exhibited similar characteristics (i.e., a hook echo on the northwestern flank of the storm as the supercell tracked to the west-southwest).

Table 1 compares the KFGZ upper-air sounding shear and stability parameters for this event with those discussed by RB98. In their baseline study of severe weather environments, they analyzed shear and stability parameters associated with the environments of ordinary cells (ORD), supercells (SUP), and tornadic supercells (TOR). These same parameters for the event discussed here indicate that at least some compare favorably with those analyzed by RB98 for the SUP and TOR categories. For example, at 0000 UTC, SRH_{0-3} compared favorably with the third quartile (Q3) while CAPE, mean shear, bulk shear, and VGP all compared favorably at the second quartile (Q2) for the SUP category. Clearly, the approach of the cold-core upper-level low resulted in enhanced shear and buoyant instability supportive of supercells—characteristics that are atypical for this region during the NAM.

4. Discussion

An unusual severe weather event with numerous supercell thunderstorms developed across portions of northern Arizona while in the midst of the warm-season North American monsoon—a regime characteristically dominated by a subtropical upper-level high over the southwestern United States. Typical conditions within the NAM include weak tropospheric vertical wind shear and nearly moist-adiabatic lapse rates. The approach of a midlatitude, cold-core, upper-level low brought an environment of enhanced shear and increased instability. These ingredients were sufficient to produce supercell storms with large hail, funnel clouds, and tornadoes. Supercells are atypical for this location at this time of the year. More typical conditions would include short-lived pulse storms that might produce small hail but are more likely to produce heavy rainfall and localized flooding. Keighton and Passetti (1998) previously documented an isolated supercell thunderstorm over northern Arizona that also occurred in an environment with a rotated hodograph. That event occurred as a midlatitude baroclinic system moved eastward across the southwest

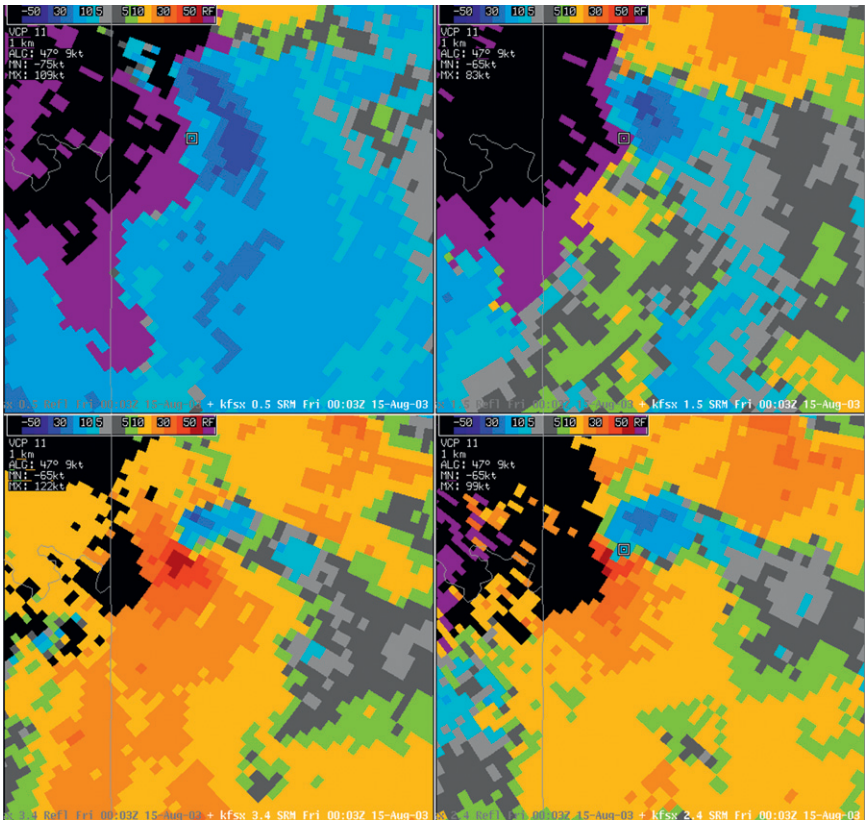

FIG. 9. As in Fig. 8, but for ground-relative velocities. Color table for velocity values is shown in the top left of each image. Negative values are inbound velocities; positive values are outbound velocities.

during the NAM transition when supercells are more likely to occur.

Model forecasts correctly showed the approach of this system many days in advance. Most forecasters recognized the enhanced potential for heavy rainfall and localized flooding; one forecaster noted a day before the event the increased shear and potential for organized storms in the Area Forecast Discussion text product.

By conducting a careful examination of the winds aloft and the shape of the hodograph—both in model forecast soundings and the actual rawinsonde data—an informed assessment of potential supercell evolution could be accomplished prior to the development of convection and supercells. As noted by Doswell (1995), being aware of the potential would increase the chances a forecaster would recognize the event as it unfolded since an important aspect of event detection is anticipation of the event. That this event was correctly anticipated is evident, in part, by the large number of severe thunderstorm and tornado warnings issued with lead time of tens of minutes. A more typical weather pattern during the NAM would see the issuance of numerous hydrological products for flooding rather than for severe thunderstorms.

Not infrequently, forecasters might expect that supercells will develop the ''classic'' characteristics of *shape* and *orientation*, even though this can only occur with the more familiar and common *curvature* and *orientation* of the hodograph [i.e., a ''synoptically evident'' event; Doswell et al. (1993)]. By properly determining, in advance, the most likely *shape*, *orientation*, and *motion* of supercell storms, the radar and warning meteorologist can focus attention on the appropriate quadrant of the

TABLE 1. Shear and stability parameters at 1200 UTC 14 Aug and 0000 UTC 15 Aug 2003 soundings taken at KFGZ. Subscripts refer to the depth in km above the ground through which the calculation is performed. The Q values in parentheses refer to the quartile to which these values compare with the results presented in Rasmussen and Blanchard (1998) for the supercell (SUP) category.

Parameter	1200 UTC	0000 UTC
CAPE (J kg^{-1})	195 (Q1)	945 (Q2)
SBCAPE (J kg^{-1})	815 (Q2)	2185 (Q4)
SRH_{0-3} (m^2 s^2)	155 (Q3)	175 (Q3)
Mean $shear_{0-4}$ ($\times 10^{-3}$ s^{-1})	6.9 (Q2)	6.7 (Q2)
Bulk $shear_{0.5-6}$ (m s^{-1})	9 (Q1)	15 (Q2)
VGP (m s^{-2})	0.1 (Q1)	0.2 (Q2)

storm to find features such as rotation aloft, hook echoes, and weak-echo regions. Bunkers and Stoppkotte (2007) likewise illustrated how a proper conceptual model of a left-moving supercell could be used to anticipate those relatively rare events.

This severe weather event served as an interesting example of an unusual environment that led to supercells having atypical orientations and motion that produced large hail, funnel clouds, and tornadoes. Situational awareness by warning and radar meteorologists—attained by a careful examination of the wind structure aloft—played an important role in recognizing the atypical supercell structure and issuing appropriate warnings.

Acknowledgements. The author wishes to thank the reviewers, in particular M. Bunkers, who provided a detailed and valuable review.

REFERENCES

Adams, D. K., and A. C. Comrie, 1997: The North American monsoon. *Bull. Amer. Meteor. Soc.,* **78,** 2197–2213.

AWS, 1961: Use of the skew *T*–log*p* diagram in analysis and forecasting. Vol. 1, AWSM 105-124, 144 pp. [Available from U.S. Air Force Air Weather Service, Scott AFB, IL 62225-5008.]

——, 1979: Use of the skew *T*–log*p* diagram in analysis and forecasting. AWS/TR-79/006 Revised, 157 pp. [Available from U.S. Air Force Air Weather Service, Scott AFB, IL 62225-5008.]

Blanchard, D. O., 1998: Assessing the vertical distribution of convective available potential energy. *Wea. Forecasting,* **13,** 870–877.

——, 2006: A cool season severe weather episode in northern Arizona. Preprints, *23rd Conf. on Severe Local Storms,* St. Louis, MO, Amer. Meteor. Soc., P3.4. [Available online at http://ams.confex.com/ams/pdfpapers/115214.pdf.]

Black, T. L., 1994: The new NMC mesoscale Eta Model: Description and forecast examples. *Wea. Forecasting,* **9,** 265–278.

Brown, R. A., 1993: A compositing approach for preserving significant features in atmospheric profiles. *Mon. Wea. Rev.,* **121,** 874–880.

Bunkers, M. J., and J. W. Stoppkotte, 2007: Documentation of a rare tornadic left-moving supercell. *Electron. J. Severe Storms Meteor.,* **2** (2). [Available online at http://www.ejssm.org/ojs/index.php/ejssm/issue/view/5.]

——, B. A. Klimowski, J. W. Zeitler, R. L. Thompson, and M. L. Weisman, 2000: Predicting supercell motion using a new hodograph technique. *Wea. Forecasting,* **15,** 61–79.

Davies-Jones, R. P., D. Burgess, and M. Foster, 1990: Test of helicity as a tornado forecast parameter. Preprints, *16th Conf. on Severe Local Storms,* Kananaskis Park, AB, Canada, Amer. Meteor. Soc., 588–592.

Doswell, C. A., III, 1991: A review for forecasters on the application of hodographs to forecasting severe thunderstorms. *Natl. Wea. Dig.,* **16** (1), 2–16.

——, 1995: Comments on "Single-Doppler radar observations of a mini-supercell tornadic thunderstorm." *Mon. Wea. Rev.,* **123,** 230–234.

——, and D. W. Burgess, 1993: Tornadoes and tornadic storms: A review of conceptual models. *The Tornado: Its Structure, Dynamics, Prediction, and Hazards, Geophys. Monogr.,* Vol. 79, Amer. Geophys. Union, 161–172.

——, and E. N. Rasmussen, 1994: The effect of neglecting the virtual temperature correction on CAPE calculations. *Wea. Forecasting,* **9,** 625–629.

——, S. J. Weiss, and R. H. Johns, 1993: Tornado forecasting: A review. *The Tornado: Its Structure, Dynamics, Prediction, and Hazards, Geophys. Monogr.,* Vol. 79, Amer. Geophys. Union, 557–571.

Houston, A. L., R. L. Thompson, and R. Edwards, 2008: The optimal bulk wind differential depth and the utility of the upper-tropospheric storm-relative flow for forecasting supercells. *Wea. Forecasting,* **23,** 825–837.

Keighton, S., and V. Passetti, 1998: Anticipation and observation of a northern Arizona supercell over high terrain. Preprints, *16th Conf. on Weather Analysis and Forecasting,* Phoenix, AZ, Amer. Meteor. Soc., 124–126.

Lemon, L. R., and C. A. Doswell III, 1979: Severe thunderstorm evolution and mesocyclone structure as related to tornadogenesis. *Mon. Wea. Rev.,* **107,** 1184–1197.

Maddox, R. A., 1976: An evaluation of tornado proximity wind and stability data. *Mon. Wea. Rev.,* **104,** 133–142.

Pytlak, E., M. Goering, and A. Bennett, 2005: Upper tropospheric troughs and their interaction with the North American monsoon. Preprints, *AMS Forum: Living with a Limited Water Supply/19th Conf. on Hydrology,* San Diego, CA, Amer. Meteor. Soc., JP2.3. [Available online at http://ams.confex.com/ams/pdfpapers/85393.pdf.]

Rasmussen, E. N., and R. B. Wilhelmson, 1983: Relationships between storm characteristics and 1200 GMT hodographs, low-level shear, and stability. Preprints, *13th Conf. on Severe Local Storms,* Tulsa, OK, Amer. Meteor. Soc., J5–J8.

——, and D. O. Blanchard, 1998: A baseline climatology of sounding-derived supercell and tornado forecast parameters. *Wea. Forecasting,* **13,** 1148–1164.

Rotunno, R., and J. B. Klemp, 1982: The influence of the shear-induced pressure gradient on thunderstorm motion. *Mon. Wea. Rev.,* **110,** 136–151.

——, and ——, 1985: On the rotation and propagation of simulated supercell thunderstorms. *J. Atmos. Sci.,* **42,** 271–292.

Thompson, R. L., R. Edwards, J. A. Hart, K. L. Elmore, and P. Markowski, 2003: Close proximity soundings within supercell environments obtained from the Rapid Update Cycle. *Wea. Forecasting,* **18,** 1243–1261.

Weisman, M. L., and J. B. Klemp, 1982: The dependence of numerically simulated convective storms on vertical wind shear and buoyancy. *Mon. Wea. Rev.,* **110,** 504–520.

——, and ——, 1984: The structure and classification of numerically simulated convective storms in directionally varying wind shears. *Mon. Wea. Rev.,* **112,** 2479–2498.

Weaver, J. F., 1979: Storm motion as related to boundary-layer convergence. *Mon. Wea. Rev.,* **107,** 612–619.

Whitfield, M. B., and S. W. Lyons, 1992: An upper-tropospheric low over Texas during summer. *Wea. Forecasting,* **7,** 89–106.

Zeitler, J. W., and M. J. Bunkers, 2005: Operational forecasting of supercell motion: Review and case studies using multiple datasets. *Natl. Wea. Dig.,* **29** (1), 81–97.

Zipser, E. J., 1977: Mesoscale and convective-scale downdrafts as distinct components of squall-line structure. *Mon. Wea. Rev.,* **105,** 1568–1589.